B25035.

AS&E

American Science and Engineering, Inc.
955 Massachusetts Avenue
Cambridge, Massachusetts 02139
617-868-1600

15 NOVEMBER 1975

ASE-3794

DATA ANALYSIS GUIDE TO THE ATM S-054 X-RAY SPECTROGRAPHIC TELESCOPE

CONTRACT NAS8-27758

PREPARED FOR:
NATIONAL AERONAUTICS
AND SPACE ADMINISTRATION
MARSHALL SPACE FLIGHT CENTER
HUNTSVILLE, ALABAMA 35812

ASE-3794

DATA ANALYSIS GUIDE to the ATM S-054 X-RAY SPECTROGRAPHIC TELESCOPE

Contract NAS8-27758

Prepared for:

National Aeronautics and Space Administration
Marshall Space Flight Center
Huntsville, Alabama 35812

Prepared by:

American Science and Engineering, Inc.
955 Massachusetts Avenue
Cambridge, Massachusetts 02139

15 November 1975

Approved: Allen S. Krieger
Allen S. Krieger
Co-Principal Investigator

TABLE OF CONTENTS

1.0 INTRODUCTION

Skylab was launched into orbit on May 14, 1973. Eleven days later its first three-man crew began a 28-day visit to the space station. The total operational life of Skylab was almost nine months and included two additional three-man visits for two and three-month periods and two unmanned intervals in which limited observations were carried out.

A major facility of the space station was the Apollo Telescope Mount (ATM) Solar Observatory, which had the capability of observing the solar atmosphere simultaneously in a spectral band covering X-rays to visible light with sufficient spatial, spectral and temporal resolution to study its structure and dynamics. This facility consisted of six instruments, one of which was the X-ray Spectrographic Telescope of our group (Experiment S-054 in Skylab nomenclature).

The S-054 X-ray telescope was a grazing incidence instrument with a spatial resolution of approximately two arc seconds on axis and sensitivity to radiation in the soft X-ray region of 2-60 Å. Crude spectral resolution within this region was achieved by means of broadband X-ray filters. A spectrographic mode of operation, employing an objective grating, was used to obtain moderate resolution spectra of flare events and of selected coronal features.

The spectroheliograph was designed around an X-ray telescope consisting of two nested grazing incidence X-ray mirrors which are both coaxial and confocal. These mirrors, developed by AS&E for ATM, employ double reflection from paraboloidal and hyperboloidal surfaces. The entrance apertures of the two mirrors were 31 and 23cm respectively, their focal length 213cm and their combined geometrical collecting area $42cm^2$. These mirrors formed the primary X-ray optics of the experiment.

The X-ray image was formed on a plane containing film from the removable camera. The film used was Kodak S0212 which is a panatomic film without topcoating but with an antistatic (Remjet) backing. Each X-ray picture is accompanied by a white light picture of the sun formed by a visible light lens positioned within the X-ray telescope. The white light image is co-aligned with the X-ray image so that information on the pitch, yaw and roll of the X-ray image can be obtained from it. Approximately 6500 frames of film were available on each film magazine. One camera magazine was used during the first (SL-1/2) Skylab mission. Two were used during the second mission (SL-3) and two magazines were exposed during SL-4. In total, approximately 32,000 solar X-ray exposures were obtained.

Exposures were taken in sequences through a given filter. This sequence was selected by a switch on the ATM console. In each case, at least 4 exposures were taken at 1/64, 1/16, 1/4 and 1 second. The sequence could be continued through exposures of 4, 16, 64 and 256 seconds. The particular setting used depended on the filter employed and on the scientific objectives of the observation. The appropriate exposure values were calculated on the basis of the results of earlier AS&E rocket flight pictures.

The spectroheliograph was designed around an X-ray telescope consisting of two nested grazing incidence X-ray mirrors which are both coaxial and confocal. These mirrors, developed by AS&E for ATM, employ double reflection from paraboloidal and hyperboloidal surfaces. The entrance apertures of the two mirrors were 31 and 23cm respectively, their focal length 213cm and their combined geometrical collecting area $42cm^2$. These mirrors formed the primary X-ray optics of the experiment.

The X-ray image was formed on a plane containing film from the removable camera. The film used was Kodak S0212 which is a panatomic film without topcoating but with an antistatic (Remjet) backing. Each X-ray picture is accompanied by a white light picture of the sun formed by a visible light lens positioned within the X-ray telescope. The white light image is co-aligned with the X-ray image so that information on the pitch, yaw and roll of the X-ray image can be obtained from it. Approximately 6500 frames of film were available on each film magazine. One camera magazine was used during the first (SL-1/2) Skylab mission. Two were used during the second mission (SL-3) and two magazines were exposed during SL-4. In total, approximately 32,000 solar X-ray exposures were obtained.

Exposures were taken in sequences through a given filter. This sequence was selected by a switch on the ATM console. In each case, at least 4 exposures were taken at 1/64, 1/16, 1/4 and 1 second. The sequence could be continued through exposures of 4, 16, 64 and 256 seconds. The particular setting used depended on the filter employed and on the scientific objectives of the observation. The appropriate exposure values were calculated on the basis of the results of earlier AS&E rocket flight pictures.

There are four modes in which the picture sequences could be taken. In the Single mode, a single sequence of 4 to 8 frames was taken with maximum exposures ranging from 1 to 256 seconds. The time between each exposure was 0.3 seconds. This mode was the one most often used in the ATM observations. In the Low mode, the selected sequence of exposures was repeated for a duration of 13 minutes. The time between individual exposures was 12 seconds. In the High mode each sequence was again repeated for a duration of 13 minutes, but with an 0.3 second interval between individual exposures. Finally the Program mode took pictures for 4 minutes at the High rate (0.3 second intervals) and for 9 minutes at the Low rate (12 second intervals). The astronaut could terminate an observing sequence or mode at any time.

To obtain detailed information on the soft X-ray spectrum, we included in the experiment an array of X-ray transmission gratings. When these gratings were placed in the optical path, either directly ahead of or behind the X-ray mirrors, the instrument became a slitless or objective grating spectrograph. For each source in the field of view, the grating-telescope combination results in a real image (or zero-order spectrum) and dispersed monochromatic images bracketing it, which include the spectra of various orders. The system has moderate spectral resolution of the grating. $\lambda/\Delta\lambda$ is of the order of 50 at 7 Å, and the dispersion in the first order is 0.5 arc minutes per Angstrom.

The AS&E experiment was also provided with a photo-multiplier counter consisting of a NaI crystal of about $5cm^2$ area and a covering window of 2 mils of beryllium. The counter operated in two modes. In the first mode, the output went through a pulse height analyzer which provided 8 channels of counts from 10 keV to 80 keV. In the second mode, the DC current was monitored and converted to a number proportional to the logarithm of the current. This number was then displayed as the PEC (photomultiplier exposure counter) on the ATM console in addition to being telemetered to ground stations. The PEC was also used as a flare warning device.

Some observations had to be made without the astronaut at the ATM console. Provisions were made for a limited number of observations made by ground command. The grating, picture rate and exposure rate could not be controlled from the ground and were set by the astronaut prior to unmanned or unattended observations. Unmanned filter selection was limited to three filters (1/2 mil Be, 1/8 mil Teflon and magazine window only). Other filter positions could only be achieved by astronaut reconfiguration of the control panel.

2.0 INSTRUMENT DESCRIPTION

A photograph of the telescope is shown in Figure 1. Figure 2 shows how the telescope was mounted to the ATM spar, the cruciform structure that provided a common platform for the ATM experiments. Figure 3 is a diagram illustrating the main features of the telescope.

Two nested coaxial and confocal grazing incidence mirror systems were used, each utilizing double reflection from a pair of paraboloidal and hyperboloidal surfaces. The optics are described in section 2.1.

2.1 The Grazing Incidence Mirrors

Two constraints severely limit the design of imaging systems for x-rays: (1) x-rays are readily absorbed by matter and (2) the index of refraction at x-ray wavelength is only slightly less than unity. For a system based on refraction, this implies a very long focal length and a very thin lens. A practical refractive system has not yet been designed. However, the fact that the index of refraction is slightly less than unity means that x-rays incident on a surface at sufficiently large angles (i.e., at grazing incidence) will undergo total external reflection. This is the basis for the design of grazing incidence x-ray imaging systems. Apart from the simple pinhole, the only other x-ray imaging device that has been used for astronomical purposes has been the Fresnel zone plate (Mollenstedt et al., 1963). Large-area zone plates are difficult to fabricate. Also, the focal length is wavelength dependent, which is a serious disadvantage for imaging a radiation source such as the corona, which consists of many discrete lines and a continuum.

Giacconi and Rossi (1960) were the first to suggest the use of paraboloidal mirrors for x-ray astronomy. By using the far zone of the paraboloid, required because of the restriction to grazing incidence reflection, paraxial rays are imaged at the focus of the paraboloid. It is not possible to satisfy the Abbe sine condition with this system, or any other single reflection system, and the image suffers from severe comatic aberration. Wolter (1952a, 1952b) demonstrated that by the addition of a second reflecting surface which is coaxial and confocal with the paraboloid, the Abbe sine condition can be approximately satisfied and comatic aberration can be reduced to acceptable limits. Wolter studied the properties of three systems which use two successive figures of revolution. The generating curves are conic sections which are concentric and have a common focal point. Most high-resolution mirrors for x-ray telescopes have been of the paraboloid-hyperboloid configuration (Figure 4). This design minimizes the problem of mechanical alignment of the two elements since the two surfaces intersect and also maximize the reflectivity for a given focal length and diameter*. The design principles for paraboloid-hyperboloid mirrors have been discussed extensively in the literature (Giacconi et al., 1969; Mangus and Underwood, 1969; Vaiana, 1974; Van Speybroeck and Chase, 1972).

The fact that an x-ray telescope is limited to grazing angles of incidence (1°-2°) results in the following practical consequences: (1) the ratio of the focal length to the diameter is large and (2) the geometrical collecting area is only a small fraction of the total polished surface area.

* Chase and Van Speybroeck (1973) have designed a mirror system of the Wolter-Schwarzschild type (Wolter, 1952b) consisting of two coaxial mirror surfaces of revolution which results in strict fulfillment of the Abbe sine rule. A quartz surface mirror system of the Wolter-Schwarzschild type has been flown by AS&E several times as part of a solar rocket payload.

In order to increase the projected frontal area of such a telescope and, therefore, to increase the speed of the system, it is possible to nest several paraboloid-hyperboloid mirrors within the available aperture. The imaging optics of the S-054 telescope consist of a nested pair of paraboloid-hyperboloid mirrors.

Figure 5 shows the mirrors in cross-section, and Figure 6 is a photograph of the mirrors. The mirror surfaces consisted of a thin layer of Kanigen, a nickel-phosphorous alloy, deposited on a beryllium support structure. Before the Kanigen deposition was applied, the support structure was machined to conform to the desired surface. The final optical figuring and polishing were performed on the Kanigen surface using conventional optical techniques*. Table I lists the mirror system characteristics.

As the diffraction limit for the mirror system is extremely small ($\sim 10^{-3}$ arc seconds for 10 Å radiation), the practical resolution was limited by attainable surface tolerances. Resolution is relatively insensitive to surface finish, and the required mechanical alignment between individual paraboloid and hyperboloid sections was easily achieved using standard mechanical procedures. Figure 7 shows the tolerances as applied to the mirror surfaces. These tolerances are specified in a way which reflects not only the necessary accuracy in the different dimensions but also the methods of measurement which were employed. Imaging tests using visible light at grazing angles are not sufficiently sensitive to surface defects, and separate measurements of surface dimensions using precision mechanical methods and optical test plates were relied upon. More complete discussions of design tolerances can be found in Vaiana (1974), Vaiana et.al. (1974a) and Giacconi et. al. (1969)

* The mirrors were manufactured by Diffraction Limited, Bedford, Mass.

Table 1

Characteristics of the S-054 X-Ray Telescope Mirrors

Focal length	213 cm
Diameter	30 and 23 cm nested pair
Geometrical area	42 cm^2
Length	34 cm
Surface Material	Kanigen
Average grazing angle	44.7 arc min. inner mirror 59.6 arc min. outer mirror
Film scale	0.001 cm/arc sec
Size of Solar Image	1.9 cm

Although the surface finish of the mirrors does not affect the resolution significantly, irregularities of the surface modify the intensity distribution in the image plane. That is, mirrors with a somewhat poor surface finish, although having high resolution, will exhibit poor acutance since a substantial fraction of the imaged power lies in the wings of the distribution. The requirements for surface finish can be specified in terms of the Rayleigh criteria for a perfect reflecting surface, which is satisfied if surface irregularities introduce errors in the reflected wavefront of less than a quarter of a wavelength. For radiation incident at a grazing angle θ, the height of a surface deviation corresponding to a $\lambda/4$ wavefront error is

$$h = \lambda/8\theta$$

For a wavelength of 8.3 Å and a grazing angle of 1°, the resulting height is 60 Å. Local irregularities with a size scale of 100-200 Å are quite evident in electron micrographs of Kanigen surfaces polished by conventional optical techniques. A substantial improvement in the surface finish of the ATM mirrors was achieved by using a chemical polishing technique* after conventional optical polishing.

Since scattering by surface irregularities modifies the distribution of focussed radiation, the spatial variation of the irradiance** in the image plane is not a true representation of the spatial variation of the radiance† of the object. We can define a point spread-function

---

*Applied Optics Center, Burlington, Mass.

**Irradiance is radiant flux density at a surface and is measured in units of energy per unit area per unit time.

†Radiance, also called specific intensity, is the fundamental radiometric quantity and is measured in units of energy per unit area per unit of solid angle per unit time.

a (x, y) for the telescope, which gives the energy per unit area per unit time at the point x, y in the image plane for a point source which yields unit energy flux density at the entrance aperture of the telescope.

The integral of the point spread function is the effective collecting area of the mirrors

$$\iint a(x, y)\, dxdy = Ar$$

where A is the geometrical collecting area of the telescope and r is the reflectivity. Now if we have an extended source of radiation which, in the absence of scattering, has an irradiance distribution in the focal plane of E(x, y), the result of the scattering is to produce a new distribution

$$E'(x, y) = \frac{1}{Ar} \iint a(\xi, \eta)\; E(x-\xi, y-\eta)\; d\xi\, d\eta$$

Thus, in order to determine E(x, y) and ultimately the source radiance distribution from the observations, the above integral must be deconvolved. The situation is further complicated by the fact that the point spread-function, both in magnitude and shape, is wavelength dependent and also depends on the position of the source in relation to the axis of the mirrors.

The point spread-function must be determined from laboratory measurements. The point-spread function of the mirrors was studied at several wavelengths between 7 Å (tungsten anode) and 44 Å (carbon anode) using a microfocus source of x-rays placed approximately 70 meters from the mirrors. The space between the mirrors and the source was evacuated. The focal plane distribution of radiation was measured using both photographic film to determine the central portion of the response function and a proportional counter provided with either a slit or a circular aperture to determine the "wings" of the function.

The on-axis point spread-function of the mirrors at 7 Å is shown in Figures 8a and 8b. There is a narrow central peak (full width at half-maximum of about three arc seconds) and rather broad wings. The narrow central peak is consistent with laboratory tests which have shown that the mirrors clearly resolve x-ray point sources 1 arc second in diameter separated by 2 arc seconds. The presence of the broad "wings" means that the power in the image spreads out over a large area. Integration of the 7 Å point-spread function shows that 50% of the power in the image is outside a radius of 48 arc seconds and that 10% of the power is more than 5 arc minutes from the image center. Since the soft x-ray radiance of neighboring features in the solar corona may vary many orders of magnitude, the significance of the point spread-function can be readily seen. Figure 9 illustrates the wavelength dependence of the point-spread function.

The effective collecting area of the mirrors is less than the geometrical projected area and is wavelength dependent. The effective collecting area at 7 Å and 44 Å has been found by summing the respective slit-scan data and also by placing a proportional counter in the focal plane to collect the total imaged radiation. Both methods give the same results. Figure 10 compares the experimental values with a theoretical curve. The experimental points fall about a factor of two below the theoretical curve; this is attributed to large-angle scattering and shadowing by surface irregularities.

2.2 X-Ray Filters

A series of filters which select broadband regions of the soft x-ray spectrum were provided in order to obtain information about the physical parameters of the solar corona. They were chosen on the basis of experience gained in a series of solar rocket flights. The sensitivity, spectral range, and dynamic range required for observations of a wide variety of solar phenomena were determined from these flights. In particular, the flights clearly identified a requirement for very thin organic filters which would allow the observation of x-rays from faint sources and at long wavelenghts (greater than 44 Å). The preparation of these filters required special techniques for fabrication, testing, and calibration.

A total of six filters was used; five were mounted on a filter wheel (Figure 11) and the sixth formed an integral part of each film magazine. The latter filter, the magazine window, always remained in the optical path and consisted of 1.2×10^{-4} cm of polypropylene ($(CH_2)_n$) coated with 2×10^{-5} cm of aluminum. This filter was made by uniformly stretching a 2.5×10^{-3} cm thick film to the required thickness and then vacuum depositing aluminum on it. An additional prefilter also remained in the optical path. This prefilter consisted of 1.4×10^{-5} cm thick aluminum foil supported by an 80% transmitting nickel mesh. The prefilter assembly (Figure 12) was situated in front of the telescope mirrors, and its primary function was to prevent unwanted ultraviolet, visible, and infrared radiation from entering the telescope.

Table 2

Characteristics of the X-Ray Filters

Filter Wheel Position No.	Material	Nominal Thickness (cm)	Measured Mass Thickness (mg/cm^2)	Pass Bands (Å)
1	Beryllium	1.3×10^{-3}	2.67	2-17
2	Teflon*(CF_2)	3.2×10^{3}	0.62	2-14; 19-22
3†				2-32; 44-54
4	Parylene-N**(C_8H_8)	5.7×10^{-4}	0.65	2-18; 44-47
5	Beryllium	5.1×10^{-3}	9.54	2-11
6	Beryllium	2.5×10^{-3}	4.72	2-14

* Du Pont Trademark
** Union Carbide Trademark
† Position 3 was left empty. The wavelength response in this position is determined by the magazine window, prefilter, and mirror reflectivity.

Table 2 lists the characteristics of the filters mounted on the filter wheel. The wavelength passbands given are for the passband given are for the 0.5% transmission points and include the effects of the reflectivity of the mirrors, the magazine window, and the prefilter.

2.3 The Objective Grating Spectrometer

To obtain detailed information on the soft x-ray spectrum, an x-ray transmission grating was included in the experiment. When this grating was placed in the optical path, the instrument became a slitless or objective grating spectrograph. This application of a transmission grating in the soft x-ray spectral region was first proposed by Gursky and Zehnpfennig (1966), and a rocket-borne telescope incorporating such a grating was flown by ASE in 1968 (Vaiana et al., 1969). For each source in the field of view, the grating-telescope combination results in a real image (or zero-order spectrum) and dispersed monochromatic images bracketing it, including several orders of the spectra. This type of system has moderate spectral resolution and is extremely efficient since all wavelengths and all sources in the field of view are examined simultaneously.

The transmission grating consisted of an array of grating elements, each consisting of parallel absorbing strips supported by a parylene-C*(C_8H_7Cl) substrate thin enough (1.2×10^{-4}cm) to be transparent to the soft x-ray range of interest. The parylene-C* substrate was first formed on a thick replica of a conventional ruled grating (1440 lines per mm) by precipitation from the vapor phase. The thin plastic layer was then stripped off and retained an impression of the grooves of the thick grating. The absorbing strips were formed on the plastic

---

*Union Carbide Trademark

layer by vacuum deposition of gold to a depth of 1000 Å. The dispersion in first order, corresponding to the grating spacing, was 0.5 arc minute per Å.

The theoretical efficiency for the grating is shown as a function of wavelength in Figure 13; the efficiency decreases at short wavelenghts because the gold becomes transparent and decreases at long wavelengths because the substrate becomes opaque. The peak at about 12 Å results from a favorable phase shift of the amplitude transmitted through the gold at that wavelength. A certain amount of gold migration occurs during the shadowing process and results in some loss of efficiency at long wavelengths. The form of the gold deposit was examined with an electron microscope. The experimental efficiency of the grating was in reasonable agreement with the theoretical calculation.

The resolving power of the grating was measured by studying its ability to resolve the tungsten M doublet at 6.74 and 6.97 A. Figure 14 shows the result obtained from a multi-element target (primarily magnesium and tungsten) masked by a slit to give the appearance of a line source. The tungsten doublet is clearly resolved in the first order. The magnesium K line at 9.89 Å is also visible. The spectral resolution, $\lambda/\Delta\lambda$, in the first order is about 50 (at 7 Å).

Twenty-four separate grating elements were fabricated in the form of annular segments to conform to the annular apertures of the mirrors. In assembling the grating, the angle between the dispersion axes of individual elements was kept to less than $\pm 1/2^{\circ}$, which was sufficiently small so as not to degrade the spectral resolution.

2.4 Camera and Film

At the time of the design and manufacture of the S-054 x-ray telescope, the selection of a suitable detection device for the x-ray images raised several questions. The only recording medium available with a resolution capability comparable to that of the x-ray telescope was film. One of the major advantages of the Skylab mission was that men were available for the first time to load and unload cameras and to return the exposed film to earth. Tests with a variety of standard film types showed Kodak Pan-X emulsion to have a suitable sensitivity to the soft-x-ray range of interest. The presence of the attenuating protective gelatin supercoat, however, limited the spectral response of the film at the longer wavelengths in the 2-60 Å range. A special unsupercoated emulsion was thus required. It was necessary to decide whether the film should be in strip or roll form. Traditionally, strip film had been used in detection systems in short wavelength spectroscopy; however, the use of roll film was both easier from the point of view of design and was more efficient from the point of view of economy of space, provided the problems of abrasion and static discharge could be overcome. After considerable design, development and testing at both AS&E and Eastman Kodak Co., a suitable emulsion was developed. This emulsion, Kodak SO 212, is an unsupercoated Pan-X emulsion on a thin Estar base with an antistatic rem-jet * backing.

The film camera used in the S-054 instrument consisted of a shutter assembly and a replaceable magazine (figure 19). Each magazine, of which there were four, had a capacity of about 356m of 70mm film,

---

*Rem jet (removable jet-black backing) is a dispersion of carbon black in a polymeric binder that is coated on the back of the base and is removed in processing.

which was enough bor about 7000 exposures. One of the magazines was reloaded in orbit with a fifth supply of film. The magazine contained a film transport mechanism and produced a set of four fiducial marks with each image to facilitate image location and aspect determination. The shutter assembly carried shutters for both the x-ray and visible light exposures. It also included a diode array which produced a photographic record of the following parameters:

a. The time at the end of each exposure, measured in days, hours , minutes, seconds and milliseconds
b. The shutter duration time
c. The frame count
d. The grating and filter configuration.

The visible light telescope system (see figure 3) had a fixed exposure time of 1/100 second duration. More flexibility in selection of exposure time was required in the case of x-ray images, since the range between the radiance of quiet features in the corona and the intense central region of a flare event can be of the order of 10^9. Thus, a series of eight different exposure durations was available, ranging in factors of 4 from 1/64 second to 256 seconds and in combination with the filters, the required dynamic range was achieved. Since it is difficult to predict the intensity of any given coronal feature, a sequence of images was always taken with a starting point of 1/64 second and with a selectable exposure range of between 4 and 8 exposures. The frequence of sequence repetitions and the interval between frames in a sequence were also variable to accommodate observations of the widely different time variations which occur in the corona.

A summary of the various camera modes and exposure sequences is shown in Tables 3 and 4 . The manual mode, single-picture rate setting, was used for most observations of quiet coronal structures and active regions, while the high, low and program picture rates were used primarily to observe flares and coronal transients. A typical day's observing program during manned operations required approximately 300 frames of film. Since a flare event required between 300 and 500 frames, only two or three such events were observed with each magazine. Figure 16 shows the film usage as a function of time. A diagram showing the configuration of an x-ray image with its associated visible light image, diode array display, and fiducial marks is shown in Figure 17 together with a portion of the exposed film from one of the magazines.

Table 3

Film Camera Operating Modes

Picture Rate	Mode-Manual	Mode-Flare Auto
Single	One sequence, high rate (0.3 second interval)	One sequence, high rate (0.3 second interval)
Low	Repeated sequences at low rate (12 second intervals) for 12.8 minutes or until stop command is issued	Repeated sequences at low rate (12 second intervals) as long as flare threshold is exceeded or until mode switch is set to manual
High	Same as low except with 0.3 second intervals	Same as low except with 0.3 second intervals
Program	First 4 minutes at high rate, then low rate of 9 minutes or until stop command is issued	First 4 minutes at high rate then low rate as long as flare threshold is exceeded or until mode switch is set to manual

Table 4

Film Camera Exposure Sequence Cycles

Exposure Range	Exposure Times (sec)	Duration of Total Sequences High Rate (sec)	Low Rate (sec)	Frames per Sequence
1	1/64, 1/16, 1/4, 1	2.5	49.3	4
4	1/64, 1/16, 1/4, 1, 4	6.8	65.3	5
16	1/64, 1/16, 1/4, 1, 4, 16	23.1	93.3	6
64	1/64, 1/16, 1/4, 1, 4, 16, 64	87.4	169.3	7
256	1/64, 1/16, 1/4, 1, 4, 16, 64, 256	343.7	437.3	8
Auto	Exposures determined by scin. detector			

2.4.1 Film Calibration

The information on the sensitometry of film in this wavelength region available to us as we began the analysis of the Skylab data was very scanty. Apart from some work which had been done in support of X-ray imaging experiments on sounding rockets, mainly at AS&E and the University of Leicester (see e.g. Atkinson and Pounds, 1964; Giacconi et al., 1969), studies of the X-ray response of film had dealt with higher energy X-rays. Accordingly it was necessary to develop the required experimental techniques in order to explore the ill-understood area of soft X-ray photographic sensitometry.

The X-ray response of the film is being studied in a laboratory program whose objective is to generate tables of net density versus deposited energy as a function of X-ray wavelength. The approach we use is to produce absolutely calibrated step wedges ("sensistrips") on film from each of the five Skylab film loads. The sensistrips are made at several wavelengths and cover the entire density range of the film, up to $D_{max} \approx 3.3$ diffuse density with about 20 energy steps. We find that the X-ray respone of the film varies slightly from roll to roll within a single emulsion batch, because of effects such as life history and, to some extent, manufacturing tolerances. In addition, there are appreciable variations in the background fog due to the space environment as well as small but non-negligible differences in the sensitometry produced by different film processing runs. Consequently, an individual calibration is required for each of the five film loads. Our progress toward this objective has involved the production of more than 150 sensistrips up to this time.

Part of the required calibration information is obtained from the analysis of 8.3 and 44 Å sensistrips prepared before the Skylab mission. These were made in identical pairs at each wavelength, one member of which was flown with each film load while the other was stored on the ground in a freezer. The members of a pair were processed together with the flight film. These strips provide information on the effects of the space environment. Additional sensistrips prepared later have been used to monitor the consistency of the sensitometry among flight film processing runs and to determine the response of the film at other wavelengths. The following discussion describes the technique used to produce the X-ray sensistrips and review the results obtained from analyzing them.

Since it is not possible to reproduce the spectrum of the million degree solar coronal plasma in the laboratory, we have adopted the approach of performing the film calibration using X-rays with selected, approximately monochromatic, wavelengths. The X-ray telescope recorded solar images through broad band filters, for the most part, so the analysis of the data does not require knowledge of the detailed wavelength dependence of the film response. It is sufficient to calibrate the film at a few wavelengths which give the average behavior over the passband of the filters.

As a practical matter, it is convenient to work with K or L characteristic lines of metals or carbon, since X-ray anodes and thin monochromatizing filters may easily be made directly from these materials. For these reasons, characteristic lines of aluminum, copper, iron, titanium and carbon at respectively 8.34, 13.3, 17.6, 27.4 and 44.7 Å were chosen (see Table 5).

The test films were exposed in a vacuum chamber, as shown schematically in Figure 18. The film was placed in a light-tight container having a rectangular thin window in front, to allow

Table 5 Materials used to generate soft X-rays

λ (Å)	Material	Energy	Filter Thickness	Transmission at Characteristic Energy	Overall Jump at Absorption Edge
8.34	Aluminum	1486 ev	5μ	0.268	191
13.3	Copper	930	2	0.040	3.5×10^{6}
17.6	Iron	705	3	0.0040	3.8×10^{11}
27.4	Titanium	452	2	0.036	2.3×10^{7}
44.7	Carbon	277	2000 Å Aluminum + 1μ Polypropylene	0.175	53

exposure of the film to a spatially-uniform flux of X-rays generated by a hot-filament/positive-anode type source about thirty inches away. Small light-trapped holes in the film container vented it during chamber pumpdown, to protect the thin window. The X-ray flux was monitored with a proportional counter, enabling us to calculate the energy deposited onto the film. An energy range of about 10^5 was covered in sixteen to twenty steps by means of varying-thickness step filters ("intensity base") at 8.3 Å and 44 Å, and by means of a movable shutter ("time base") at all wavelengths. Comparisons of intensity-base and time-base results at 8.3 and 44 Å wereused as a partial check on the consistency of our energy calculations.

Mechanically, the light-tight containers, called "sensitometers", are built to hold strips of film 70 mm wide by about 14 inches long, and consist of three parts: the main body, an insert containing the light-tight thin window, and a light-tight back. The film is held emulsion side forward, about 1/2 inch behind the window. For 8.3 Å, the functions of light-tight window and step filters are combined in a series of overlapping layers of 0.00025-inch aluminum foil, arranged to provide a sequence of steps each 5 mm wide. The thirty inch distance between the source and the film provides sufficient collimation so that there is negligible shadowing at the step boundaries. For 44.7 Å, the thin window is approximately one micron of stretched polypropylene onto which 2000 Å of aluminum has been vacuum deposited to make it light proof. The step filter consists of layers of stretched polypropylene, each two microns thick, which gives a transmission of about 0.6 per step. The edges of the steps are not straight, but are catenary shaped, to avoid flow of the polypropylene as it ages or if its temperature changes. The step filter is clamped to the front of the sensitometer, directly outside the aluminized window.

The monochromaticity requirements on the X-rays are not stringent. Characteristic K or L lines from solid targets have inherently small widths, but the electrons hitting the anode also generate bremsstrahlung X-rays in addition to the characteristic line. The bremsstrahlung constitutes a background covering the entire range from very low energy up to the energy corresponding to the anode voltage. It is necessary to filter out this bremsstrahlung at wavelengths other than the desired line. This is done by making the light-tight window of the same material as the anode, e.g., aluminum foil for an aluminum anode, stretched polypropylene for carbon. The thin windows have sharp transmission maxima at wavelengths just slightly greater than that of the characteristic lines due to the K (or L) absorption edges, and thus act as monochromatizing filters.

The anode voltage at which the source is operated affects both the X-ray flux and the purity of the spectrum. As the voltage is increased the output flux of the characteristic line increases strongly. At the same time the cut-off in the bremsstrahlung spectrum moves to higher energies at which the filter transmission is greater. Because the bremsstrahlung emission spectrum falls off for photon energies approaching the anode voltage, there is some flexibility in choosing the anode voltage. For each wavelength a maximum voltage was chosen based on an assessment of tolerable spectral contamination by higher energy bremsstrahlung versus the desirable counting rate.

The time required to make a sensistrip whose densest step approaches D_{max} is a function of the flux. With our apparatus, it varies from a few hours at 8.3 Å to some weeks at 17.6 Å. The time for the latter wavelength is reduced in practice by not going all the way out to D_{max}, but rather, cutting off in the shoulder region of the characteristic curve. This reduces the time required to only one week of continuous running.

The response of the film is given in the form of H-D curves, in which the diffuse density is plotted against the logarithm of the X-ray energy deposited. X-ray H-D curves, like those for visible light, have well differentiated toe, straight line, and shoulder regions. The slope of the straight line portion, γ, is one of the experimental parameters describing the characteristic curve. The energy where this straight line intercepts the background density level is a measure of the speed of the film. In our work, we use the speed parameter, "$a\mu$", defined as $0.5616/E_o$, where E_o is the energy of the intercept, and the proportionality 0.5616 comes from a model which will be discussed in the last section. The other parameters describing the H-D curves are D_b, the background density level, and D_{max}, the maximum net density. For our purposes, the actual film base density and the chemical fog produced in processing are lumped together in D_b. The film calibration tables are generated from $a\mu$, γ, D_b and D_{max} by computer program. Therefore, our calibration effort has been concerned with determining these four parameters for each of the five Skylab film loads as a function of X-ray wavelength.

The response of the film is, of course, affected by the space environment. Table 6 gives the fog levels for the Skylab film loads. The effects are an increase in the density in the toe region, a decrease in γ, and a reduction of density in the shoulder region. The latter effects are associated with a loss of developable grains in the emulsion; that is, a loss in film speed. Sensistrips made at 8.3 and 44 Å were flown with each flight film load and are used to eliminate the effects of background fog from the density to energy conversion. Figures 19 and 20 show some sensistrips made in matched pairs at 8.3 and 44 Å, one member of each pair on fogged film and one on unfogged film. The effect of defogging is

Table 6 Fog levels in the ATM flight film loads

Magazine	Film Base and Chemical Fog	Additional Net Fog Due to Space Environment
A	0.11	0.03
B	0.11	0.11
C	0.11	0.11
D	0.11	0.23
E	0.13	0.08

qualitatively the same in both cases, although of course we see that the overall shape of the curve depends on the wavelength involved. Figure 21 shows a graph of $D_{\text{fogged film}}$ vs $D_{\text{unfogged film}}$ at 8 and 44 Å, drawn from the data of Figures 4 and 5. The same straight line fits the data at both wavelengths in the linear region. Thus, a linear correction is satisfactory, i. e.,

$$D_{\text{fogged}} = \alpha D_{\text{unfogged}} + \beta$$

where D_{unfogged} is the density produced on unfogged film by a given X-ray exposure, D_{fogged} is the density on fogged film due to the same exposure, and α and β are constants independent of wavelength. Microdensitometer scans of flight film are corrected to give corresponding unfogged densities without consideration of the spectrum of the original incident radiation.

The parameters of the sensitometric curves depend strongly on the details of the development of the film. The shoulder region is especially sensitive to processing chemistry. The developer replenishment rate must be carefully matched to the total amount of silver being reduced, which varies from magazine to magazine because of different fogging levels. In order to obtain the required large dynamic range in the solar photographs, our films were developed to give visible light γ of about 1.4. Development was 7.5 minutes in D96 at 68 °F, in a modified ciné-type processor. Excellent uniformity of the sensitometry was achieved, as for three of the runs shown in Figure 22

Our main results are the behaviors of γ and $a\mu$ as functions of X-ray wavelength as shown in Figures 23 and 24 for one of the Skylab film loads. Figure 23 shows γ vs wavelength and Figure 24 $a\mu$ vs wavelength. The error brackets reflect the range of uncertainty in determining γ and $a\mu$ from sensistrips as well as the statistical variations present even among sensistrips exposed and developed together.

An effort to produce a model for the film response (Van Speybroeck, 1969) resulted in an expression which has been used quite successfully as a four-parameter fit to the experimental H-D curves. The model was derived from arguments based on the amount of energy deposited locally in a region of the emulsion. The derivation ignored many factors, especially the development chemistry and it is no surprise that the film response predicted by the model is only qualitatively correct. However, quantitative reproduction of the data is obtained by adjusting the parameters of the model empirically.

The gross diffuse density, D, corresponding to X-ray energy deposition is given by:

$$D = D_b + D_{max} \left[1 - \frac{1}{\mu t} Ei(a\mu E) + \frac{1}{\mu t} Ei\left(a\mu E e^{-\mu t}\right) \right]$$

where D_b, D_{max}, $a\mu$ and $\mu t = (2.3 D_{max})/\gamma$ are the parameters whose values are obtained from experimental data. The notation Ei represents the exponential integral:

$$Ei(z) = \int_z^{\infty} \frac{e^{-x}\,dx}{x} .$$

The expression is in suitable form for evaluation by computer. Values of reduced x^2 well below unity are achieved routinely on a scale where $x^2 = 1$ corresponds to an uncertainty in density of about 0.01 to 0.02. For example, Figure 25 shows a comparison of experimental and computer fitted points. The x^2 of the fit is 0.7. Thus, the model can be used, together with the experimental data on the wavelength dependence of the $a\mu$ and γ shown in Figures 23 and 24 to interpolate between H-D curves measured at different wavelengths. The parameters D_b and D_{max} are independent of wavelength. Figure 25 also may be taken to represent the goodness of fit of the computer-generated curves to the experimental results that would be expected if the interpolated H-D curve could be compared with an experimental sensistrip at the same wavelength. The two curves agree well everywhere, although not as well in the shoulder region and toe-to-center transition region as elsewhere.

2.4.2 Film Processing

To provide for the proper development of this film it was necessary to choose the target sensitometry, and to establish tolerances on the process sensitometry to achieve a high degree of photometric control. An acceptable variation in density for a sensitometric exposure was defined as ± 0.03 diffuse density units throughout the D log E curve. The tolerance imposed on departures from the target gamma was ± 0.06. With these stringent requirements on the processing sensitometry the photometric accuracy would be assured.

It was obvious from the development tolerances, the quantity of the film, and the physical handling requirements, that a suitable processing machine would have to be procured. There are basically two different types of wet development from which to choose: immersion or spray development. It was felt that an immersion development system would more easily provide the processing reliability that was called for. Some of the other factors involved in the final design of a processor were the total number of processing steps, the throughput speed, and the overall physical size of the machine.

The approach taken to meet the strict development tolerances was one of overwhelming brute force: using a very large volume of developer in order to minimize the magnitude of changes in such parameters as temperature and chemical composition. The ratio of film area to developer volume was approximately 34 cm^2 of film per liter of developer. The remainder of the processing steps are designed to exceed the requirements for archival permanence of the photographic image.

The recommended developers for 3400, the "parent" of SO-212, were originally D-19 and D-76 and more recently Versamat Type A chemistry. The D-19 and Type A chemistries were designed to produce a high gamma required for high altitude aerial photography where the inherent image brightness range is low. Our imagery, on the other hand, has a very high brightness range, necessitating a lower gamma process. The brightness range of the "quiet" sun is approximately 10^3 as illustrated in Figure 26. With a solar flare in the field of view, this range can increase to 10^5 or 10^6. Kodak's D-96 developer that has been used in the motion picture field for many years, is a so-called negative developer designed for machine processing. With this developer we could easily achieve a γ in the range of 1.2 to 1.6. These values of γ give the desired photometry consistent with the exposure variations that were programmed into the instrument aboard Skylab. Processing this film to the maximum gamma achievable would undoubtedly increase the energy resolution, but would have reduced the photographic usefulness of the data.

The approach used to monitor the constancy of the development process was twofold: sensitometry and chemical analysis. The sensitometers were a Kodak Model 101 Sensitometer for the visible light sensitometry and soft X-ray sensitometers of our own design for the various monochromatic X-ray wavelengths (as discussed in a companion paper, Simon et. al., 1974). The chemistry parameters monitored were the developer pH and the concentration of potassium bromide, which was found to be a necessary adjunct to sensitometry in determining the proper replenishment rate for a given average density on the film. With this process control, development consistency was achieved throughout each of the five 1300 ft. rolls of film.

An added complication of the process control was not being able to develop all five rolls at the same time. As shown in Table 7 the first roll was processed in June of 1973, rolls 2 and 3 were processed in October 1973, roll 4 in February 1974 and roll 5 in March 1974. Each of these processes was done in a fresh batch of chemicals, preceeded by the appropriate calibration runs to verify the reliability of the machine and the chemistry. It was found that by controlling the other development parameters very closely, such as temperature to $\pm$ 0.3 F, development time

Table 7

PROCESS CONTROL FOR S054 FLIGHT FILM
VISIBLE LIGHT SENSITOMETRY

MAGAZINE LOAD NO.	PROCESSING DATE	DENSITY VALUES FOR $\Delta LOGE=1.0$ LINEAR REGION OF CURVE		GAMMA
#1	JUN 73	.76	2.10	1.34
#2	OCT 73	.81	2.21	1.40
#3	OCT 73	.78	2.18	1.40
#4	FEB 74	.78	2.24	1.44
#5	MAR 74	.80	2.21	1.41

to $\pm$ 1.5%, and maintaining the agitation rate at a moderately high and consistent level, we were easily able to attain the very high processing standards we set for ourselves.

2.5 Photoelectric Detection Systems

The primary instrument of the S-054 experiment was the photographic x-ray telescope described in the preceding sections. Two secondary photoelectric x-ray detection systems were also provided to assist the Skylab crewmen in operating the telescope and to obtain complementary high-energy x-ray data during flare events.

The first of these systems was a scintillation detector consisting of a NaI(Tl) crystal, a 14-stage photomultiplier, and associated electronics. The crystal was 2.5cm in diameter and 1.0cm thick. A thin, .05cm beryllium window was bonded to the front face of the crystal. The combination of window, bonding material, and a thermal shield limited the low energy response of the detector to x-rays with energies greater than 1.5 KeV. On the high energy side, the crystal detection efficiency dropped below 50% at 120 KeV. The detector, which measured the x-ray flux density from the whole solar disc, had two simultaneous modes of operation. In the first mode, the photomultiplier output pulses corresponding to energies greater than 10 KeV were sorted by means of an eight-level pulse height analyzer. In the second mode, the average DC level from the photomultiplier was monitored. This signal was also the input to an audio and visual flare alarm system to alert the astronauts to the occurrence of a flare on the sun.

The second photoelectric detection system was an x-ray "finder" telescope. This unit consisted of a small x-ray mirror (7.6cm diameter, 81cm focal length) mounted coaxially with the primary telescope mirrors and an x-ray image dissector. Figure shows a block diagram of the system. A 0.0125cm thick CaF_2(Eu) scintillation crystal was bonded to the face plate of the image dissector tube and was located at the focal plane of the small mirror. This crystal served as an x-ray to visible light converter and was optically coupled to the photocathode of the image dissector tube by means of fiber optics.

In this experiment, the image dissector signal was used to modulate a cathode-ray tube display; the deflection plates of the image dissector and cathode-ray tubes were driven synchronously, and thus a real-time image of the sun was obtained. Approximately one second was required for a complete image scan with a resolution of one arc minute. The cathode-ray tube was located on the astronauts' ATM control and display panel in the multiple docking adapter of Skylab. Using the display, an astronaut could locate a flare event and point the telescope to within one arc minute of its position.

2.6 Thermal Control and Electronics Systems

In addition to the telescope assembly, the experiment also included a main electronics assembly and a thermal control assembly. Commands to the experiment and telemetry data from the experiment were processed through the main electronics assembly. The electronics assembly was mounted separately from the telescope assembly on the ATM supporting structure. The thermal control assembly was mounted near the telescope on the ATM spar.

The overall power requirements were 100 watts average, 140 watts peak at 28 volts. The largest items in the power budget were the thermal control assembly (50 watts average, 78 watts peak) and the main electronics assembly (31 watts, average and peak).

The scientific data available on telemetry included the following: scintillation detector output, image dissector count, picture count (a record of frames expended); X-ray exposure duration; camera shutter status; filter wheel position; grating position, ATM pointing information (pitch, yaw and roll).

Housekeeping data were also telemetered to ground. These data included: temperatures at four locations in the telescope assembly and two in the camera assembly; and power supply high and low voltages.

The thermal control system was designed to maintain the telescope assembly at $70 \pm 2^{\circ}F$, assuming a nominal ATM canister temperature of $55^{\circ}F$. It was fully redundant with primary and secondary control loops.

Since long intervals of the Skylab mission were unmanned, provision was made for limited operational capability by means of ground command. Grating position, picture rate and exposure range could not be controlled by this means and had to be pre-set by the astronaut. However, exposure sequences could be initiated or terminated, and filters 1, 2 and 3 could be selected by ground command.

3.0 SCIENTIFIC OBJECTIVES

The scientific objectives of the S-054 experiment which guided the pre-mission planning and mission operations provide the framework for the analysis of the data. The initial phases of the data reduction and analysis program have also produced refinements in the emphasis and the approach to the tasks. The scientific objectives were formulated in a list of thirty-four Problem Objectives which were discussed in detail in ASE-3242.

In 1975 the emphasis of the work has been on the morphological studies of a variety of topics. The morphological work is a necessary preparation for and companion to quantitative analysis. The latter requires a fairly elaborate system of programs, program packages, and catalogs which are continuously being developed and updated. While the complete development of a system with the necessary complexity is a long term effort, substantial quantitative work is possible now. In the coming year further improvements will aid in the performance of this analysis both for scientists in the S-054 group and guest investigators from outside institutions.

The following is a summary of the objectives which have been and are being pursued and which will be the focus of our future work. The topics include:

A. The emergence of magnetic field into the corona from lower levels and the birth of coronal features.

B. The reconnection and dispersion of the magnetic field.

C. The fundamental flare process and the mechanisms for plasma heating, the release of stored energy, and cooling of the flare plasma.

D. The magnetohydrodynamics of the inner corona represented by the transformation of the finely structured photospheric and chromospheric magnetic fields into the large scale fields of the outer corona and interplanetary medium.

E. The temperature and density distributions in coronal features and their evolution, including changes associated with transients.

F. The relation between coronal structures and the solar cycle.

G. The relationship between the structures of the inner corona and the solar wind.

The Joint Observing Program (JOP).

The ATM experimenters as a group, developed a number of observing programs designed to study specific solar features or phenomena and hence to investigate specific problems in solar physics. In general, relevant ATM instruments observed the same feature either simultaneously or sequentially during the performance of a JOP. The JOP's were subdivided into a series of mission objectives (MO) which took the form of specific observational techniques or of feature subclassifications. Each MO was then made up of a succession of fundamental observing sequences or Building Blocks. In designing the Building Blocks an attempt was made to select the operating modes of each experiment which were particularly suited to a given type of observation, such as spatially resolved observations of faint or bright features, flare observations, etc.

An additional advantage gained from the coordinated JOP approach was the relative ease with which the daily observing program and near-real time changes to that program could be made. It also made possible a much wider range of coordinated observations. While it was generally beneficial for the five ATM experiments to take simultaneous observation of solar features of phenomena, the scientific value of the data increases still further if accompanied by simultaneous ground based observations. For instance, observations of an active region are greatly enhanced if, at least, corresponding Hα, CaK, magnetic field and microwave radio observations are also available.

For further information on mission operations see the ATM Experiments Reference Book, NASA LBJ Space Center, EVA & Experiments Branch, Crew Procedures Division (1973).

3.1 Morphological Analysis

Visual inspection of X-ray images provides information on the three-dimensional structures present in the solar corona. The lifetimes of various features can be examined and their evolution described qualitatively as they cross the solar disc. The outline of flare structures can be determined and their evolution throughout the flare rise, flare fall, and post-flare phases can be determined.

Characteristic dimensions can also be obtained from the images. It is of considerable interest to know the range of sizes of X-ray active regions, coronal flux tubes, and structures associated with filaments and prominences.

Comparisons can also be made with other solar data. The X-ray features can be compared with ground-based magnetograms, H α, Ca K, etc. and with other space observations, such as the Skylab XUV, UV and white light coronal data obtained simultaneously with the X-ray data.

In order to provide the photographic medium best suited for a particular scientific investigation, we have developed an extensive photographic facility. Five major forms of photographic presentation are currently produced for these investigations. They are:

a. Contact reflection prints. The purposes of the reflection prints, high-quality "proof prints", are to give a subjective representation of the information content of the original images and to provide a "quick look" at the data for the selection of images for further photographic presentation.

b. Magnified (5x) images on transparent intermediate nagative ("Interneg") film stock with an information content comparable to that of the original film. These enlarged 2P's (second generation, positive image) are used for detailed morphological studies.

c. Wide dynamic range, unity magnification, film copies. These are used with an optical viewer for evaluation of time variations, the lifetimes at various features, and for the detection of new coronal phenomena.

d. High-quality reflection prints (5x) produced from "Internegs". These presentations, because of the limitations of photographic paper, have a smaller dynamic range than presentations (b) and (c). However, the exposure and contrast may be selected to display a feature of interest in an optimum manner.

e. Motion picture films. These are used to illustrate the evolution of features or events, short-term structural changes, etc.

Figure 27 illustrates the sequence of production of the various presentations. A more comprehensive discussion of the preparation of the photographic material can be found in the paper by Haggerty et al. (1974). The contact reflection prints can be thought of as high quality proof prints. Aside from the fact that it is imperative to minimize the use of the original film, there is a much more basic photographic problem. The density range of the imagery is exceptionally high. In a given exposure, there is useful information at densities close to base plus fog all the way up to density values of approximately 3.2 The saturation density of the film for the process that was used is 3.3, as shown in Fig. 28. It is well known that the maximum useful density range that can be printed on a photographic paper is

b. Magnified (5x) images on transparent intermediate negative ("Interneg") film stock with an information content comparable to that of the original film. These enlarged 2P's (second generation, positive image) are used for detailed morphological studies.

c. Wide dynamic range, unity magnification, film copies. These are used with an optical viewer for evaluation of time variations, the lifetimes at various features, and for the detection of new coronal phenomena.

d. High-quality reflection prints (5x) produced from "Internegs". These presentations, because of the limitations of photographic paper, have a smaller dynamic range than presentations (b) and (c). However, the exposure and contrast may be selected to display a feature of interest in an optimum manner.

e. Motion picture films. These are used to illustrate the evolution of features or events, short-term structural changes, etc.

Figure 27 illustrates the sequence of production of the various presentations. A more comprehensive discussion of the preparation of the photographic material can be found in the paper by Haggerty et al. (1974). The contact reflection prints can be thought of as high quality proof prints. Aside from the fact that it is imperative to minimize the use of the original film, there is a much more basic photographic problem. The density range of the imagery is exceptionally high. In a given exposure, there is useful information at densities close to base plus fog all the way up to density values of approximately 3.2 The saturation density of the film for the process that was used is 3.3, as shown in Fig. 28. It is well known that the maximum useful density range that can be printed on a photographic paper is approximately 1.5. It would therefore take three different exposure levels on the paper to record the full density range of a single original image.

A much more logical approach would be to compress the original density range in one or more photographic steps on film. A pair of companion films, Eastman Fine Grain Duplicating Positive 5366 and Eastman Fine Grain Duplicating Negative 5234 appeared to possess the necessary characteristics, as shown in Fig. 29. The sequence in which we use the films is opposite to their normal usage, that is, we use the low gamma 5234 as the master positive and then print back to 5366 as the duplicate negative. By processing the 5234 to a gamma of approximately 0.55 and the 5366 to a gamma of approximately 1.4 we achieve a product gamma of approximately 0.77, which when multiplied by the original density range yields a printing negative with a density range of approximately 2.2, as shown in Fig. 30. Attempting to further reduce the density range of the printing negatives would result in a sacrifice of contrast in the toe region of the original image that is too great.

We are better able to tolerate a loss of information content of the highlight regions of the long exposure images because there are other images of lesser exposure levels in a camera sequence designed to record the brighter regions of the sun. Therefore, the reproduction process is tailored more toward the low density areas of the original image.

The image size of the solar disk on the original film is slightly under 2cm in diameter. To do any meaningful visual morphological analysis this image must be photographically enlarged to a more workable size. The magnification we chose as a standard yielded a disk of 10.8 cm in diameter for exposures taken on 1 June 1973. This magnification also has the added convenience of allowing the use of a standard 8 x 10 sheet of photographic material to record the full image including the extended corona.

These enlarged 2 P's (second generation, positive image) compress the large density range of the original image to a photographically more usable value. The material selected for the enlarged 2 P's is Kodak Professional Copy Film 4125. This film has a unique D log E curve; it is a compound curve with two distinct slopes. In the high density part of the curve the slope is steeper, having a gradient of 1.7 compared with a gradient of 0.45 for the low density end. The value of this curve is twofold: it enhances the apparent contrast of the low density parts of the original image and it compresses the overall density range. Enlarger flare also helps to some extent in compressing this density range. In producing the enlarged 2 P's the exposure and processing parameters are controlled very closely, so that the base plus fog region of the original film produces a target density on the 4125 of 2.0 ± 0.05. The D_{MAX} regions of the original film are reproduced at a density of approximately 0.15. Thus, we have an enlarged film positive which reproduces nearly all of the detail of the original image in a much more manageable density range. From this point, using conventional photographic processes, we can produce high quality reflection prints, slides, motion pictures or whichever photographic medium is best suited for a particular scientific investigation.

3.2 Quantitative Data Reduction and Analysis

The methods by which coronal plasma parameters, such as electron temperature and density as a function of position, are determined from the x-ray images will be discussed in this section.

The x-ray images are scanned by a Photometric Data System Model 1010A microdensitometer with an aperture of 20 micrometers (2 arc seconds). The resulting digitized density arrays are stored on magnetic tape. Approximately one hour is required to scan the full solar disc. The density arrays are converted into digitized irradiance arrays (the distribution of energy per unit area per unit time deposited on the film) by means of the film calibration curves and a correction for fog. Since the film is wavelength dependent and the incident wavelength distribution is not known a priori, this procedure is an iterative one. In principle these arrays should be deconvolved in order to remove the effects of telescope scatter. In practice, at the present time, deconcolution is only done for special purposes. Without deconvolution in a number of cases, it is still possible to obtain useful information about the temperature and density structure of various coronal features.

In order to relate the focal plane irradiance distribution to the coronal parameters, a quantitative relationship between the radiation emitted by the corona and that imaged by the telescope is required. Details of this process can be found in Vaiana, et. al (1975).

3.3 INFORMATION FOR NSSDC USERS

3.3.1 Note on Quantitative Analysis

Every reasonable effort has been made to insure that the copy film sent to the NSSDC is of the highest quality possible, both photographically and photometrically. However, there is an inevitable degradation in resolution and in sensitometry involved in any copy step. We have found that quantitative work must be performed with the original flight film and strongly urge users of copy films not to attempt quantitative analysis from these images. The images can be used for morphological work such as is performed by the S-054 team, again with the caution that the original will always contain more information than any copy.

The flight original is kept in a secured, environmentally controlled area at American Science and Engineering in Cambridge, Mass. Anyone wishing to perform quantitative analysis using the S-054 data should contact Dr. G.S. Vaiana at the Center for Astrophysics or Dr. A.S. Krieger at AS&E.

3.3.2 The Film Image Catalog

All of the prime bookeeping data for the S-054 experiment are contained in concise form in the Film Image Catalog (FIC). An up-to-date copy of the catalog is included with the film and this report. It gives essentially complete data for all five S-054 film magazines; any errors are of a minor nature and should not affect the user.

The FIC is to be used with the film, and contains for each image, such data as the exposure time, filter, exposure duration, aspect and various housekeeping data associated with the ATM/JOP program. The sources for the FIC are camera operations converted from the light diode array on the film, manual bookkeeping data acquired real-time during the Skylab Mission and aspect data from telemetry downlink.

Fig. 31 shows a sample page from the FIC listing, 22 columns of data are present. Cross-indexing from the film itself is provided via the Frame ID number in Col. 1. The Frame ID consists of the magazine letter code prefix (A-E for the 5 magazines) and a 4-digit number which is identical to the last 4 digits of the number on the film. The FIC magazine letter code prefix is related to the 2-digit film code prefix through Table 8 . A suffix letter, usually 'S', is provided to distinguish between the few duplicate frome numbers that occured during the numbering of the film.

Cols. 3 and 4 give the calendar date and Greenwich Mean Time (UT) to the nearest second at the <u>end</u> of that frame's exposure. Col. 6 gives the exposure duration in seconds of the image. Most of these times are in multiples of 4 (see Table 4) for the nominal exposure duration plus a fractional part for the transit time of the shutter blades across the FOV. Magazine E exposure times are different because the shutter was disabled. Occasionally throughout the FIC, an exposure was terminated abnormally either by the astronaut or by ground command. Col. 7 is the filter number (1 to 6) and Col. 8 tells whether the objective grating was in (I) or out (O). Cols. 4-8 are the data taken from the diode array (see Sec. 2.4)

Cols. 9-13 are bookeeping data logged real-time during the mission. Col. 9 gives the Picture Data Mode (see Table 3). Col. 10 gives the Daylight Pass No., or the orbit no., numbered monitorically for every 90 min. Skylab orbit for each of the these manned missions. Cols. 11 and 12 are the JOP and BB ID's for the particular referenced S-054 sequence (see Sec. 3.0). Col. 13 identifies the nominal pointing location on the solar disc of the ATM optical axis (and the S-054 axis). Table 9 is the code for the abbreviations in Col. 13. The numbers refers to the NOAA/Boulder nomenclature.

The telemetry downlink aspect data is contained in Cols. 14, 15 and 17. Cols. 14 and 15 contain the pitch (garn X) and you (garn Y) coordinates offset from sun center in arc seconds. Col. 17 is the roll reference angle in degrees (0 to $\pm$ 180°). The aspect quantities are discussed further in Sec. 3.3.4.

Col. 2 contains up to 7 "Special Status Indicators" which are defined in Table 10 . Cols. 16 and 18-20 are computer housekeeping data for the FIC.

Table 9

FIC Frame No.	Film Frame Number
A XXXX S	71 XXXX
B XXXX S	72 XXXX
C XXXX S	73 XXXX
D XXXX S	94 XXXX
E XXXX S	05 XXXX

Note: when the film is right-reading, i.e. Solar Image has North up, East to the left, the emulsion is down and the film frame numbers will be reversed.

Table 9

SC	Sun Center
AR	Active Region
FP	Filament
PP or PR	Prominence
QR	Quiet Region
NC	Network Cell
LS	Limb Scan
CH	Coronal Hole
LB	Limb
SI	Solar Inertial
BS	Bright Spot
SCOX, COMET, etc.	Special Targets of Opportunity such as Scorpius X-1, Comet Kohoutek, etc.

Table 10

FIC FORM1 REPORT

FIELD	EXPLANATION OF SPECIAL STATUS INDICATORS
FRAME	"*" BEFORE THE FRAME INDICATES THE 1ST OF A SEQUENCE
FRAME FLAGS 1234567	(1) "I" INDICATES THAT AN INTERNEG HAS BEEN MADE (2) "U" DEFINES UNMANNED PERIOD OF OPERATION (2) "M" DEFINES MANNED PERIOD OF OPERATION (3) "A" MEANS THAT OUTSIDE SOURCE ASPECT ALIGNMENT HAS BEEN DONE FOR THIS FRAME (4) "D" MEANS THAT A TELEMETRY ASPECT DATA DROPOUT OCCURED DURING ASPECT COMPUTATION (5) "E" MEANS THAT TELEMETRY ASPECT DATA POINTS WERE ELIMINATED DURING THE ASPECT COMPUTATION (6) "F" INDICATES THAT THE VALUE OF THE ASPECT PARAMETERS FOR THIS FRAME DIFFER FROM THE AVERAGE ASPECT CALCULATED FOR THE ENTIRE SEQUENCE. (7) CURRENTLY UNUSED
GAMX GAMY GAMRR	THE FIELD SUFFIX CHARACTERS ARE DEFINED AS FOLLOWS: "*" IMPLIES THAT THE CORRESPONDING ASPECT POINTING PARAMETER WAS NOT TOTALLY STABLE DURING THE EXPOSURE. THE EXPOSURE MAY BE "BLURRED" AND THE ASPECT SHOULD BE CHECKED. AN "*" IS PRINTED WHEN THE STANDARD DEVIATION FOR THE PARAMETER IS GREATER THAN: 3.00 ARCSEC FOR GAMX & GAMY 0.10 DEGREES FOR GAMRR "*" INDICATES THAT THE CORRESPONDING PARAMETER WAS MANUALLY ENTERED INTO THE FIC CATALOG.
GAMRR	THE FIELD SUFFIX CHARACTERS ARE DEFINED AS FOLLOWS: "I" INDICATES THAT GAMRR CAME FROM AN IBM SOURCE "T" INDICATES THAT |GAMRR(IBM -TELEMETRY)| > 1 DEG. "V" INDICATES THAT GAMRR HAS BEEN VERIFIED CORRECT
XY-CHG	DATE THAT GAMX OR GAMY WAS LAST CHANGED IN THE FIC
RR-CHG	DATE THAT GAMRR WAS LAST CHANGED IN THE FIC.

3.3.3 Anomalies Affecting The Data

Some hardware problems occured during the 9 months of the mission which affected the S-054 data. The first photographs with the telescope were taken on May 28, 1973; and 5 days later, on June 2, the ATM cannister aperture door in front of the telescope failed closed. For the next five days the door remained closed, although telemetry signals falsely indicated that the door was jammed open. Because of this signal, 1500 frames were transported but unexposed, hence the data gap appearing in the FIC between June 2-8. On June 7 the Skylab crew performed an EVA (Extravehicular Activity) and pinned the door open. It remained open for the rest of the mission.

Problems occurred with the canister rate gyros which caused the experiment Pointing Control System to be turned off for two periods of several days each with the result of degraded imagery due to the poorer stability of the Solar Inertial System. These periods were between manned missions, July 16-29 and Nov. 15-19, and are indicated by 'SI' in the FIC.

On November 27 the filter wheel failed in position 5, the location of the thickest filter. S-054 operation continued; however, the exposures taken during the failed period showed only features with relatively high surface brightness. This filter remained in the optical path until December 25, when the crew during an EVA moved the wheel permanently to position 3, the blank position on the filter wheel.

During the work on the filter wheel, the camera shutter was damaged to the extent that the shutter blade permanently obscured a portion of the telescope field of view. An additional result was to reduce the effective flux reaching the film by about a factor of 4. The unknown amount and geometry of the obscuration renders detailed quantitative reduction of Magazine E data nearly impossible. However, the absence of a shutter permitted very long exposure allowing observations of coronal limb structures further out from the solar limb than for any other magazine.

On all magazines but A, the one-second exposure occassionally appears as a double image. This is due to a defect in the camera take-up mechanism and never effected any other exposure The 1-second image is still useful for morphological study of flares and active region cores, but quantitative analysis is difficult.

3.3.4 Data Selection - Use of the FIC and the film

This section is an overview of some practical technique the user should employ for use of the S-054 data. The data consists of the FIC (see Sec. 3.3.2) and the film. Typically the user will look first in the FIC for those frames or sequences of frames which will be most useful for his analysis. Combinations of frames by time, filter, exposure duration and grating in or out are typically used. The user might, for example, want to examine all filter 3, 64 second frames, grating out approximately every 6 hours for a specified period. When the user locates these, he records the frame numbers and finds them on the film using the magazine conversion in Table 8

Occasionally the user may want to check the diode array pattern on the film, if, say, he feels an error may exist in the diode array data contained in the FIC. Fig. 32a shows the pattern orientation if the film is right-reading (emulsion down). The rows are indicated by letters and the 6 columns by numbers. The time data (GMT) is contained in rows A-E and rows F-K contain data for the grating position, filter, picture counter, and exposure duration. The filled spaces represent reference dots in the pattern that are always "on". Fig. 32b gives an example and is self-explanatory. The coding of the three-dot filter pattern is shown in Table 11. The last item needed for a description of the use of the data is the aspect. The telemetry aspect in the FIC is known to be inaccurate for precise alignment of any two images that were taken many minutes or hours apart. Following is a brief discussion of the ATM pointing system and its anomalies. Several references provide a detailed summary of the aspect system (see, for example, "Skylab and The Sun" (1973), Chubb (1970), MSFC Report (1974)). I give here only a brief outline of the system and its performance including the major anomalies which were encountered.

Table 11

Filter Code

C	B	A	Filter
0	0	0	1
0	0	1	2
1	0	1	3
1	0	0	4
1	1	0	5
0	1	0	6
1	1	1	T

The ATM instruments were hard-mounted to a cruciform spar enclosed in a canister. The canister was fine pointed to areas on the solar disk by the Experiment Pointing Control(EPC) system. The EPC consisted conceptually of 3 systems: the Fine Sun Sensor (FSS) for pitch and yaw pointing accuracy and stability; the roll positioning system for roll pointing and stability; and the electronic, mechanical and computer interfaces for the system.

The heart of the FSS system was an optical encoder system. The system was designed such that when sun centered, a null signal was output from a detector that sampled the two halves of the solar image. Offset pointing capability came from optical wedges which, when rotated, forced the detector to move the canister to again null the signal. The pre-mission spec on the pointing accuracy of the FSS was ± 2 1/2 arc-sec over a ± 24 arc min offset from sun center with a stability of ± 2 1/2 arc sec over 15 min in time and a jitter of 1 arc sec/sec. Post mission results indicate the FSS system maintained these specs very well throughout the mission.

The major pointing problems during the mission occurred in the roll determination system. The heart of this system was a star tracker which provided the only absolute reference for determination of solar north when it was actively tracking a star. Unfortunately, several problems caused the star tracker to be used infrequently during the mission. Absolute roll determination was then usually unknown and the estimated roll was dependent on knowledge of the spacecraft drift and the orbital plane error (precession of the orbital plane) between times of star tracker usage. Details of the "reconstruction" of the roll reference after the mission are contained in IBM(1975). Star tracker problems which led to its limited usage included false tracking of spacecraft contaminants entering the FOV, the shutter sticking open, photomultiplier tube degradation probably due to the shutter problem and failure of the gimbal system, which prevented star tracker usage near the end of the mission. The result was that star tracker usage required crew intervention and was performed only every few hours because of scheduling difficulties.

The pre-mission roll specs were $\pm$ 10 arc min in pointing accuracy, ~10 arc min over 15 min stability and a jitter of $\pm$ 3 arc min/sec. The stability values were achieved but the absolute roll reference (knowledge of solar north) was degraded because of the above factors. Post mission reconstruction by IBM (1975) improved the roll reference accuracy to an average of about $\pm 2^{\circ}$ as determined by comparison with outside data sources such as the S-054 ATM white light star fields and ground-based H_{α} photos.

Precise alignment for solar north, then, is impossible by using just the ATM aspect data. We have found that accuracies of $\pm 1^{\circ}$ can be achieved by carefully overlaying same-scale transparencies of an X-ray image and an H_{α} image with solar north marked on it. For best results, these images should be within minutes or an hour or so of each other. Once north is marked on the X-ray image, alignment between pairs of X-ray images can proceed in the following manner.

For full disc, filter 3 images that are taken within about 8 hours of each other, the smallest visible bright features, called "X-ray bright points", can be used for coalignment. 9 hours is the mean lifetime of those features. The large scale structure, such as active regions and coronal holes should not be used for accurate alignment since these features evolve on a time scale of hours. For coaligning images further apart in time than 8 hours, the user must either align each image with an Hα image or align X-ray image pairs using small features near the solar poles where the effect of solar rotation will be minimized. For even crude coalignment of evolving features within small areas of the disc, like flares, the user must remember to include an area large enough such that independent features can be used for the alignment.

REFERENCES

1. Atkinson, P.A. and Pounds, K.A.: 1964, J.Photo. Sci. 12, 302.

2. Chase, R.C. and Van Speybroeck, L.P.: 1973, Appl. Opt. 12, 1042.

3. Chubb, W.B.: 1970, in Optical Telescope Technology, NASA SP-233, p.437

4. Giacconi, R. and Rossi, B.: 1960, J. Geophys. Res. 65, 773.

5. Giacconi, R., Reidy, W.P., Vaiana, G.S., Van Speybroeck, L.P., and Zehnpfennig, T.F.: 1969, Space Sci. Rev., 9, 3.

6. Gursky, H. and Zehnpfennig, T.: 1966, Appl. Opt. 5, 875.

7. Haggerty, R., Simon, R., Golub, L., Silk, J.K., Timothy, A.F., Krieger, A.S. and Vaiana, G.S.: 1974, Soft X-ray Imaging on Photographic Film, to be published in AAS Photo-Bulletin.

8. Henke, B.L. and Elgin, R.L.: 1970, Advances in X-ray Analysis, vol. 13, Plenum Press, New York

9. Krieger, A.S., Paolini, F., Vaiana, G.S., and Webb, D.: 1972, Solar Phys. 22, 150.

10. Mangus, J.D. and Underwood, J.H.: 1969, Appl. Opt. 8, 95.

11. Möllenstedt, G., Van Grote, K.H., and Jonsson, C.: 1963 in X-ray Optics and X-ray Microanalysis, Third International Symposium, Stanford, 1962 (ed. by H.H. Pattee, V.E. Cosslett and A. Engström), Academic Press, New York, p. 73.

12. MSFC Skylab Mission Report: Saturn Workshop; NASA TMX-64814 Oct. 1974., p. 6-1ff.

13. Poletto, G., Vaiana, G.S., Zombeck, M.V., Krieger, A.S. and Timothy, A.F.: 1975, A Comparison of Coronal X-ray Structures of Active Regions with Magnetic Fields Computed from Photospheric Observations, to be published in Solar Phys.

14. Silk, J.K., Kahler, S.W., Krieger, A.K., Vaiana, G.S.: 1975, Time Changes in the Structure and Spectrum of an X-ray Flare, Bul. AAS 7, 355

15. Simon, R., Haggerty, R., Golub, L., Krieger, A.S., Silk, J.K., Timothy, A.F., and Vaiana, G.S.: 1974, presented at the AAS Working Group on Photographic Materials, 18-20 August 1974, Rochester, New York. "Response of Photographic Film to Soft X-ray Radiation".

16. Skylab And the Sun, NASA, July 1973, Primarily p. 18

17. Tucker, W. H., and Koren, M.: 1971, Ap. J. 168, 283.

18. User's Guide for Reconstructed Roll References(γ_{RR}): IBM, March 31, 1975.

19. Vaiana, G.S., Reidy, W.P., Zehnpfennig, T., Van Speybroeck, L., and Giacconi, R.: 1969, Science 161, 564.

20. Vaiana, G.S.: 1974, "Methods of Imaging X-ray Astronomy and the X-ray Spectroheliograph on ATM" CNES Space Optics, Proceedings of the Summer School on Space Optics, Marseilles, 1970, eds. A. Marechal and G. Courtes, Gordon and Breach Pub., New York City, pp. 295-338.

21. Vaiana, G.S., Krieger, A. and Timothy, A.F.: 1973a, Solar Physic. 32, 81.

22. Vaiana, G.S., Davis, J.M., Giacconi, R., Krieger, A.S., Silk, J.K., Timothy, A.F. and Zombeck, M.: 1973b, Ap. J. 185, L47.

23. Vaiana, G.S., 1972, 1970 CNES Space Optics, Proceedings of the Summer School on Space Optics, Marseilles, Gordon and Breach Publishers, Paris.

24. Vaiana, G.S., Krieger, A.S., Petrasso, R., Silk, J.K. and Timothy, A.F.: 1974a, in Instrumentation in Astronomy-II, Proc. of the Soc. Photooptical Instrumentation Engineers, 44, 185.

25. Vaiana, G.S., Krieger, A.S., Timothy, A.F., and Zombeck, M.: 1974b, ATM Observations, X-ray Results, to be published in Space Sci. Reviews

26. Vaiana, G.S., Van Spreybroeck, L.P., Zombeck, M.V., Kreiger, A.S., Silk, G.K. and Timothy, A.F., 1975 submitted to Space Science Instrumentation.

27. Van Speybroeck, L.P. and Chase, R.C.: 1972, Appl. Opt. 11, 440.

28. Van Speybroeck, L.P.: 1969, Internal Memorandum, AS&E December 1969.

29. Wolter, H.: 1952a, Ann. Physik, 10, 94.

30. Wolter, H.: 1952b, Ann. Physik, 10, 286.

FIGURE CAPTIONS

Figure 1	Photograph of the X-ray telescope. The prefilters were not mounted on the front aperture plate when the photograph was taken.
Figure 2	Drawing showing the X-ray telescope mounted to the ATM spar. Five other major instruments were mounted to the spar.
Figure 3	Functional diagram of the X-ray telescope.
Figure 4	Paraboloid-hyperboloid X-ray telescope mirror configuration.
Figure 5	Cross-section of the X-ray telescope mirrors.
Figure 6	Photograph of the X-ray telescope optics showing the nested 30 and 23cm mirrors. The small telescope, which focuses an X-ray image on an image dissector, can be seen reflected from the curved surface of the 23cm diameter paraboloid.
Figure 7	Surface tolerances on each dimension of the X-ray mirrors. R is the radius, ΔR is the difference in radii of the two ends, and S (x) is the nominal surface profile.
Figure 8a	The point spread function of the telescope out to 15 arc minutes for 7 Å radiation.
Figure 8b	The point spread function of the telescope near the image center for 7 Å radiation.
Figure 9	Scans of images to illustrate the wavelength dependence of the point spread function. The images were lines a few arc seconds wide and about ten arc seconds long. The images were scanned with a proportional counter masked by a

split a few arc seconds wide and about 15 arc minutes long. The 7 Å curve has been normalized to match the 44 Å curve at the image center.

Figure 10 The theoretical wavelength dependence of the effective area of the telescope for an on-axis source. The vertical scale on the right is the effective area divided by the geometrical area. The experimental points fall about a factor of two below the calculated values.

Figure 11 Filter wheel

Figure 12 Prefilter assembly

Figure 13 Calculated first-order efficiency of the grating as a function of wavelength. The efficiency is defined as the fraction of the incident power sent into the spectrum.

Figure 14 A spectrogram of a laboratory source of X-ray radiation produced by the transmission grating. The source target anode was composed of tungsten and magnesium. The tungsten M_α and M_β lines at 6.97 Å and 6.74 Å respectively, are clearly resolved in first order. The magnesium K line at 9.89 Å is visible in first and second order.

Figure 15 Film magazine. Each replaceable magazine, of which there were five, had a capacity of about 356m of 70mm film.

Figure 16 The total number of frames exposed on each day of the Skylab mission.

Figure 17 A diagram showing the configuration of the film and a photograph of a portion of the exposed film.

Figure 18 Schematic overall view of laboratory setup for generating sensistrips.

Figure 19 Matched 8.3 Å sensistrips showing effects of fogging by the space environment. The circles represent data on unfogged film, the squares, fogged film.

Figure 20 Matched 44 Å sensistrips showing effects of fogging by the space environment. The circles represent data on unfogged film, the squares, fogged film.

Figure 21 Plot of density on fogged film versus density on unfogged film at corresponding energies. Circles are points at 8.3 Å, triangles at 44Å. Original data is from Figures 4 and 5. Both sets of points may be fitted with one straight line:

$$D_{FOG} = +.93\, D_{NO\ FOG} + 0.12.$$

Figure 22 Typical H-D curves at 8.3 Å for three film loads, each processed in a separate run.

Figure 23 Experimental values of γ vs λ.

Figure 24 Behavior of speed a_μ as a function of wavelength-linear plot.

Figure 25 Comparison of experimental points with a computer-fitted line.

Figure 26 Soft x-ray photographs of the solar corona obtained from Skylab during the operation of the Apollo Telescope Mount solar observatory on 1 June 1973. The X-ray bandpass of both images is 2-32, 44-54Å (a) is a 256 sec. exposure, (b) is a 0.255 sec exposure. When comparing two images whose exposures differ by a factor of approx. 1,000 it can be seen that the brightest feature in the short exposure image has a density equivalent to some of the dimist features, thereby demonstrating in the long exposure image; an intrinsic brightness difference in the soft x-ray corona of at least 10^{-3}.

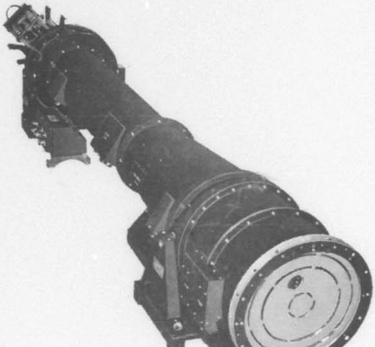

Fig. 1

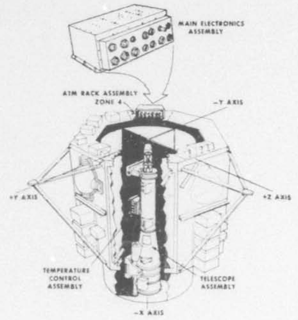
MAIN ELECTRONICS ASSEMBLY
ATM RACK ASSEMBLY ZONE 4
-Y AXIS
+Y AXIS
+Z AXIS
TEMPERATURE CONTROL ASSEMBLY
TELESCOPE ASSEMBLY
-X AXIS

Fig. 2

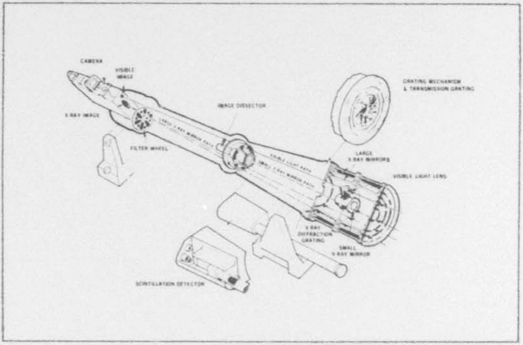
CAMERA
VISIBLE IMAGE
X-RAY IMAGE
FILTER WHEEL
IMAGE DISSECTOR
GRATING MECHANISM
& TRANSMISSION GRATING
LARGE X-RAY MIRROR PATH
VISIBLE LIGHT PATH
SMALL X-RAY MIRROR PATH
LARGE X-RAY MIRRORS
VISIBLE LIGHT LENS
X-RAY DIFFRACTION GRATING
SMALL X-RAY MIRROR
SCINTILLATION DETECTOR

CONFOCAL HYPERBOLOID
PARABOLOID
REFLECTING SURFACES

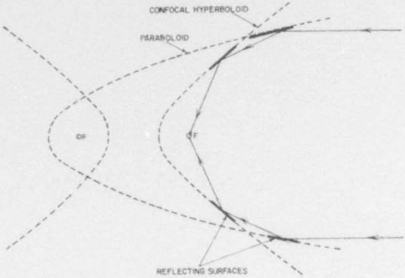

CONFOCAL HYPERBOLOID
PARABOLOID
F
F
REFLECTING SURFACES

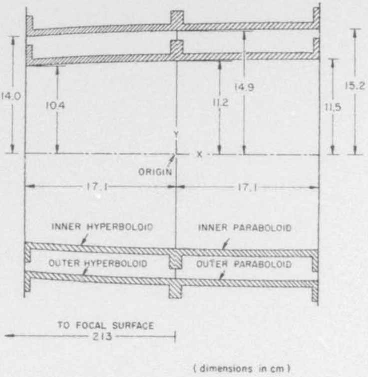
14.0
10.4
14.9
11.2
11.5
15.2
Y
X
ORIGIN
17.1
17.1
INNER HYPERBOLOID
INNER PARABOLOID
OUTER HYPERBOLOID
OUTER PARABOLOID
TO FOCAL SURFACE
213
(dimensions in cm)

Fig. 5

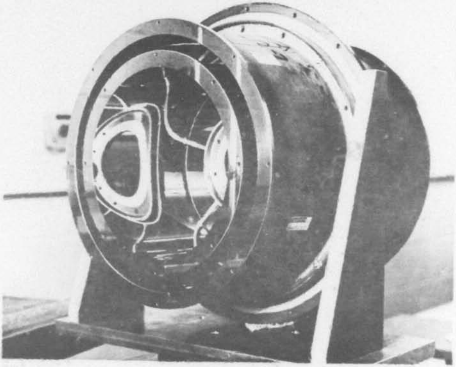

Fig. 6

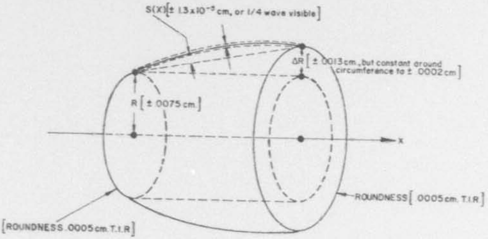
S(X)[± 1.3 x 10⁻⁵ cm, or 1/4 wave visible]
ΔR [± .0013 cm., but constant around circumference to ± .0002 cm]
R [± .0075 cm.]
x
ROUNDNESS [.0005 cm. T.I.R]
[ROUNDNESS .0005 cm. T.I.R]

Fig. 7

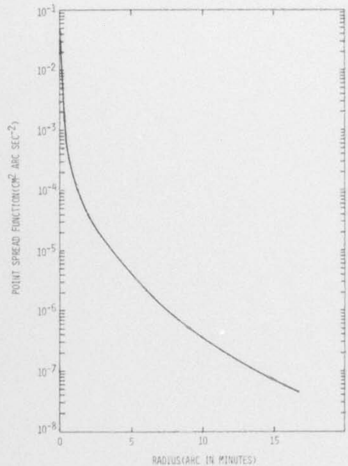

POINT SPREAD FUNCTION(CM2 ARC SEC-2)
10-1
10-2
10-3
10-4
10-5
10-6
10-7
10-8
0
5
10
15
RADIUS(ARC IN MINUTES)

Fig. 8a

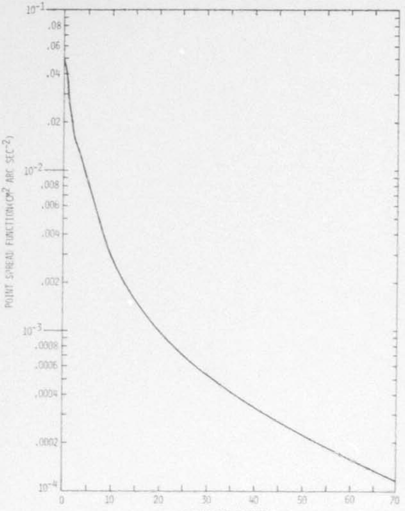

10^-1
.08
.06
.04
.02
10^-2
.008
.006
.004
.002
10^-3
.0008
.0006
.0004
.0002
10^-4
0
10
20
30
40
50
60
70
RADIUS(ARC SECONDS)
POINT SPREAD FUNCTION(CM^2 ARC SEC^-2)

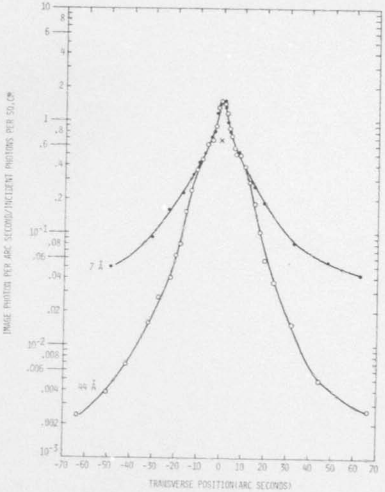

IMAGE PHOTON PER ARC SECOND/INCIDENT PHOTONS PER SQ.CM
TRANSVERSE POSITION(ARC SECONDS)
7 Å
44 Å

Fig. 9

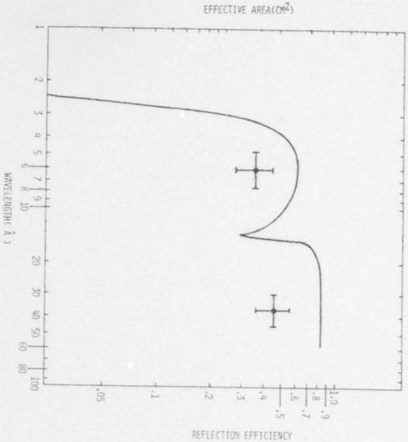

Fig. 10

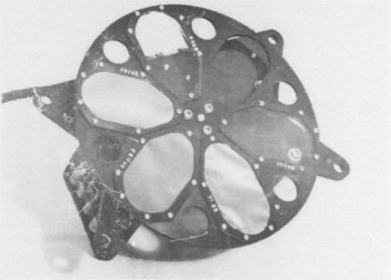

Fig. 11

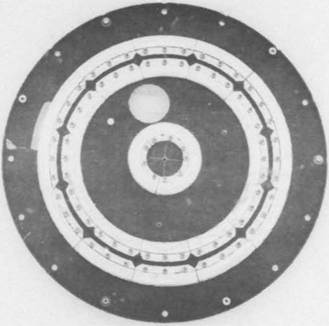

Fig. 12

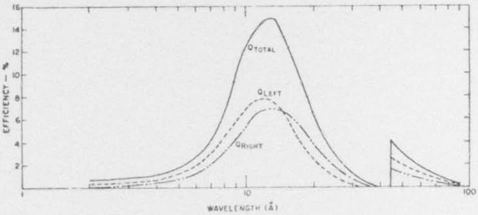
16
14
12
10
8
6
4
2
EFFICIENCY — %
Q TOTAL
Q LEFT
Q RIGHT
1
10
100
WAVELENGTH (Å)

Fig. 13

Fig. 14

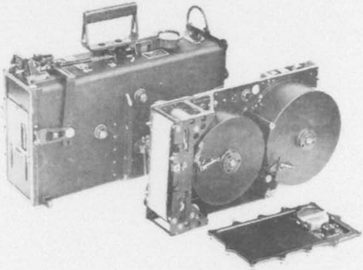

Fig. 15

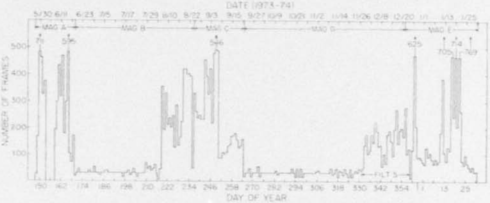
DATE (1973-74)
5/30 6/11 6/23 7/5 7/17 7/29 8/10 8/22 9/3 9/15 9/27 10/9 10/21 11/2 11/14 11/26 12/8 12/20 1/1 1/13 1/25
MAG A
MAG B
MAG C
MAG D
MAG E
FILT 5
NUMBER OF FRAMES
100
200
300
400
500
150 162 174 186 198 210 222 234 246 258 270 282 294 306 318 330 342 354 1 13 25
DAY OF YEAR

Fig. 16

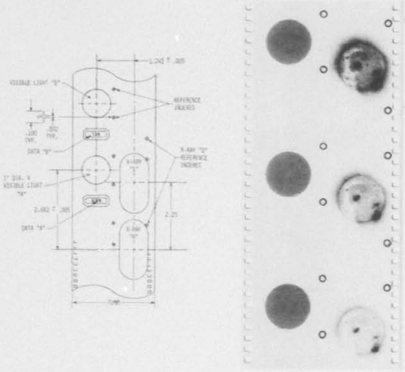
1.242 ± .005
REFERENCE
INDEXES
.200
TYP.
.002
TYP.
X-RAY
2.482 ± .005
2.25
70MM

Fig. 17

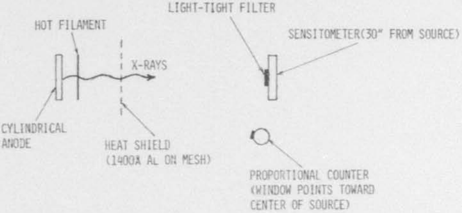

SCHEMATIC OVERALL VIEW OF LABORATORY SETUP FOR GENERATING SENSI-STRIPS

Fig. 18

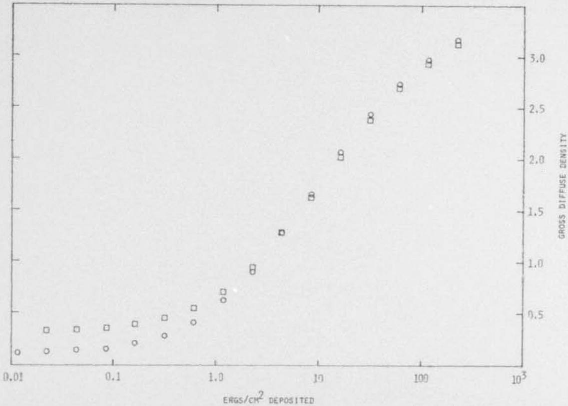
3.0
2.5
2.0
1.5
1.0
0.5
GROSS DIFFUSE DENSITY
0.01
0.1
1.0
10
100
10^3
ERGS/CM^2 DEPOSITED

Fig. 19

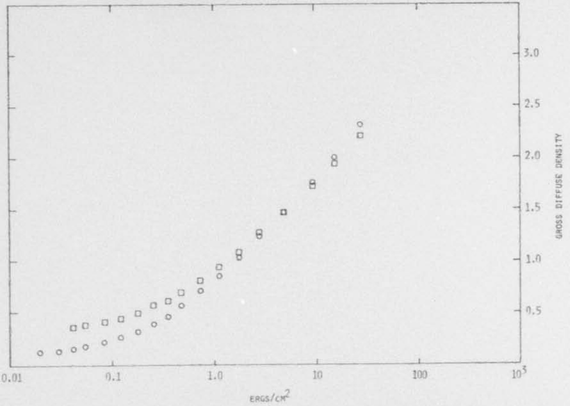

0.01
0.1
1.0
10
100
10^3
ERGS/CM^2
3.0
2.5
2.0
1.5
1.0
0.5
GROSS DIFFUSE DENSITY

Fig. 20

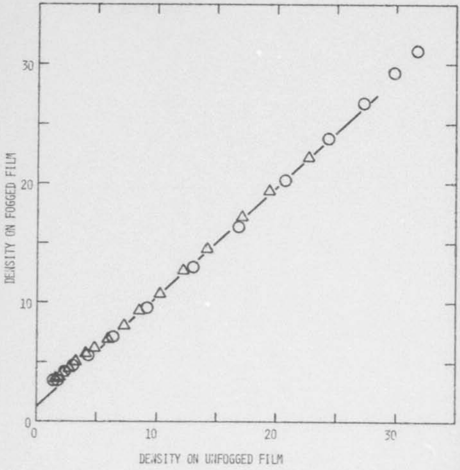

Fig. 21

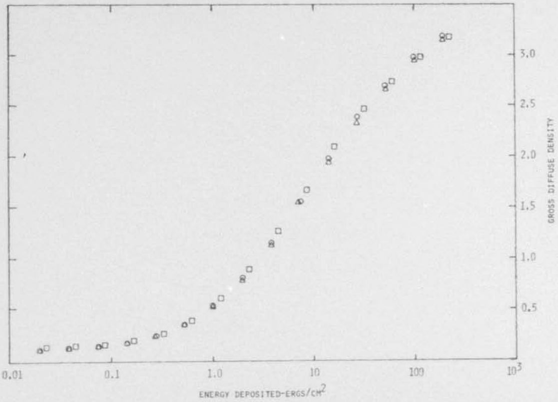
3.0
2.5
2.0
1.5
1.0
0.5
GROSS DIFFUSE DENSITY
0.01
0.1
1.0
10
100
10^3
ENERGY DEPOSITED-ERGS/CM^2

Fig. 22

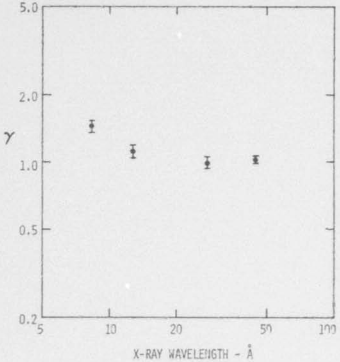

EXPERIMENTAL VALUES OF γ VS. λ .

Fig. 23

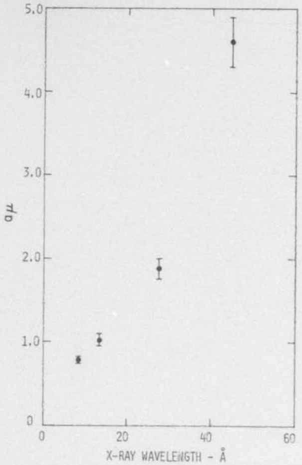

BEHAVIOR OF SPEED $a\mu$ AS A FUNCTION OF WAVELENGTH (LINEAR PLOT)

Fig. 24

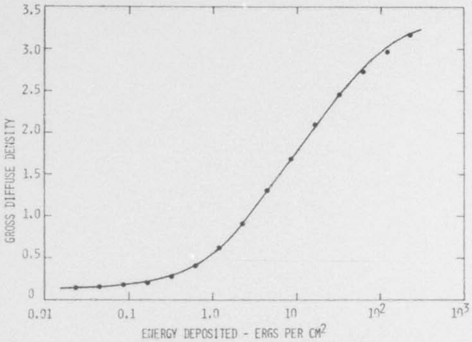

COMPARISON OF EXPERIMENTAL POINTS WITH A COMPUTER FITTED LINE

Fig. 25

a.

b.

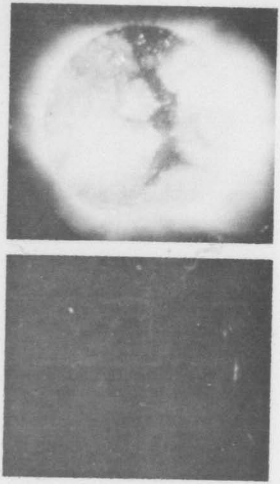

Fig. 26

PHOTOGRAPHIC IMAGE PROCESSING

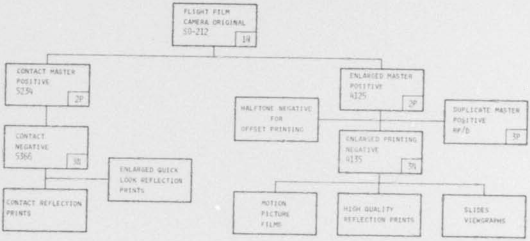

Fig. 27

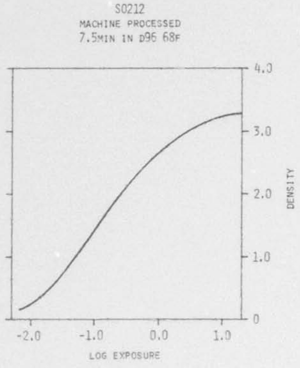
SO212
MACHINE PROCESSED
7.5MIN IN D96 68F
4.0
3.0
2.0
1.0
0
DENSITY
-2.0
-1.0
0.0
1.0
LOG EXPOSURE

Fig. 28

DUPLICATING FILMS
MACHINE PROCESSED
3.75 MIN IN D96 75F

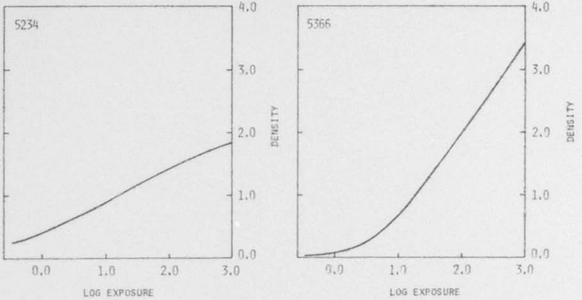

Fig. 29

REPRODUCTION CURVE

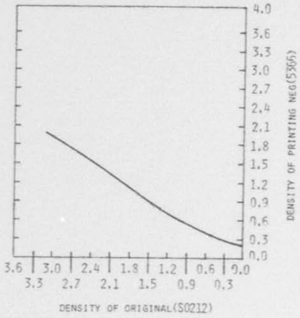

Fig. 30

AISI SKYLAB AT#/S-056 PACSRA#

***** PIC MYCAMIN REPORT - LISTIC IN SEQUENCE (FRAME ORDER) *****

[illegible]

Fig. 31

DIODE ARRAY CODE AS VIEWED
ON READER VIEWING SCREEN

						L
		GRATING	FILTER C	B	A	K
512	256	BINARY 128	PICTURE 64	32	16	J
8	4	COUNTER 2	EX- 1	256	64	H
16	4	-POSURE 1	RANGE 1/4	1/8	1/16	G
EXP. 1/32	1/64					F
	32	G M T - 16	DAYS 8	4	2	E
DAYS 1	16	8	HOURS 4	2	1	D
32	16	MINUTES 8	4	2	1	C
32	16	SECONDS 8	4	2	1	B
500	250	MILLISECONDS 125	62.5	31.2	15.6	A
6	5	4	3	2	1	

Fig. 32a

GRATING OUT, FILTER 3

FILM COUNTER = 275

EXPOSURE DURATION = 64.05SEC

G M T

9 DAYS

12 HOURS

19 MIN.

12 SEC.

516 MSEC.

Fig. 32b